International Journal of Heat and Mass Transfer 57 (2013) 285–291

Contents lists available at SciVerse ScienceDirect

International Journal of Heat and Mass Transfer

journal homepage: www.elsevier.com/locate/ijhmt

Enhanced cooling for LED lighting using ionic wind

Ing Youn Chen [a], Mei-Zuo Guo [a], Kai-Shing Yang [b], Chi-Chuan Wang [c,*]

[a] Department of Mechanical Engineering, National Yunlin University of Science and Technology, Yunlin 640, Taiwan
[b] Green Energy and Environment Research Labs, Industrial Technology Research Institute, Hsinchu 310, Taiwan
[c] Department of Mechanical Engineering, National Chiao Tung University, Hsinchu 300, Taiwan

ARTICLE INFO

Article history:
Received 2 August 2012
Received in revised form 29 September 2012
Accepted 3 October 2012
Available online 8 November 2012

Keywords:
Electrohydrodynamics
Ionic wind
LED
Natural convection

ABSTRACT

This study employs ionic wind to augment heat transfer of a LED mounted on a substrate. The size of the LED chip is 0.9 mm × 0.9 mm with a nominal power of 1 W. A needle type electrode is used to generate ionic wind with the applied voltage ranging from 4 to 11 kV. The effects of aligned angle, electrode polarity, separation distance, and ground configuration on the thermal resistance of the LED substrate are examined in this study. For the same applied voltage, it appears that the thermal resistance for the negative polarity is lower than that for the positive one and the negative electrode also has a wilder operation range. The thermal resistance can be reduced as much as 50% in the test range. The thermal resistance is slightly reduced when the aligned angle is increased from 0° to 20°, but a further increase of aligned angle casts no further reduction on the thermal resistance. It is found that the influence of vertical separation distance between the needle and ground electrode is moderately higher than that of horizontal separation distance. Test results also indicate that the mesh ground electrode shows moderately lower thermal resistance than those of point or line electrode.

1. Introduction

Thermal management is one of the most important issues to ensure operational stability of LED lighting applications, and it becomes more severe when the power is further increased. Currently high-power, high-brightness LEDs had penetrated into almost every aspect of lighting applications [1,2]. High-power LEDs in operation can produce high luminance, but they also generate significant heat at the same time. The heat raises severe problems to maintain a low LED die temperature. It had been reported that the optical output of the LED is sharply degraded with the increase in junction temperature [3] because the high temperature significantly influences the reliability and durability of the LED [3–5]. In contrast to other lighting sources; radiation heat transfer barely contributes to heat dissipation for LED due to its relatively low die temperature as relative to an incandescent lamp [6]. Hence thermal management of LEDs depends mainly on both conduction and convection heat transfer. The former, which determines the thermal resistance from LED junction to substrate, plays essential role in spreading heat from a tiny LED die to its packaging substrate, while the latter is mainly responsible for the heat transfer from substrate to ambient [7].

Cooling of LED is primarily via convection and conduction. The latter involves heat spreading across the bonding interface [8,9]. In common implementation of LED cooling with regard to convection, passive methods incorporating natural convection heat sinks such as plate fin and radial fin (e.g., [10,11]) are the mostly adopted methods. In addition, some active methods are also available in heat removal, such as microjet array cooling system for cooling of a high-brightness LED array [12,13], liquid-cooling system, thermoelectric cooler, and oscillating heat pipes are also feasible techniques that efficiently dissipate heat out of the high power LEDs [14–17]. Though the foregoing active methods show effective heat removal in high power LEDs, concerns of noise and vibration for these active methods remain. Therefore, rather than using mechanical devices to promote airflow for active cooling, the forced convection can also be implemented without any moving part such as using an electro-hydrodynamic (EHD) approach, where no rotational or moving mechanism is involved. This would certainly simplify the design and manufacture of cooling module for LED devices.

Forced convection derived from ionic winds had been discovered for more than a century. It was not until in the 1960s did the ionic winds came into notice as a means for thermal management. There had been intensive studies focusing in using the EHD technique to augment the heat transfer performance of the heat sinks under natural convection (e.g., [18–21]). The previous efforts aimed at macro scale heat transfer augmentation under natural convection. Notice that the size of LED die is rather small and

* Corresponding author. Address: E474, 1001 University Road, Hsinchu 300, Taiwan. Tel.: +886 3 5712121x55105; fax: +886 3 5720634.
E-mail address: ccwang@mail.nctu.edu.tw (C.-C. Wang).

0017-9310/$ - see front matter © 2012 Elsevier Ltd. All rights reserved.
http://dx.doi.org/10.1016/j.ijheatmasstransfer.2012.10.015

Nomenclature

A	proportional constant for Townsend like relation for positive polarity, A volt^{-2}	Q_a	actual heat dissipation, W
A^+	proportional constant for Townsend like relation for positive polarity, A volt^{-2}	Q_l	heat loss from the bakelit, W
A^-	proportional constant for Townsend like relation for negative polarity, A volt^{-2}	R	electrical resistance, Ω
E	electric field, V m^{-1}	R_{th}	thermal resistance, °C W^{-1}
H	height, mm	RH	relative humidity, %
i	corona current, μA	T	temperature, °C
h	height of the electrode (relative to substrate), mm	$T_{ins,c1}$	measured temperature at the top of the bakelite, °C
k	thermal conductivity, W m^{-1} K^{-1}	$T_{ins,c2}$	measured temperature at the bottom of the bakelite, °C
L	length, mm	ΔT	temperature difference between LED and ambient, °C
P	power, W	V	applied voltage, volt
Q	rate of heat transfer, W	V_0	threshold voltage, volt
		dx	distance between the measured temperatures on the bakelite, °C
		θ	aligned angle, °

normally possess an extraordinary spreading resistance. In this regard, it would be beneficial to employ EHD near the LED die for effective lifting of the magnitude of the spreading resistance. Hence it is interesting to examine the influence of electrode arrangements, such as aligned angle, distance, and ground electrode configuration on the thermal resistance of the LED chip. The objective of this study is to clarify the effect of relevant parameters of such EHD system.

2. Experimental apparatus and data reduction

The experimental setup consisting of an environmental chamber, a LED die attached on a ceramic substrate, and a power supply system, as well as a data acquisition system, is schematically shown in Fig. 1a. In order to maintain a constant and uniform ambient temperature throughout the chamber without any fan during the experiment, an environmental chamber having a volume of 0.5 m

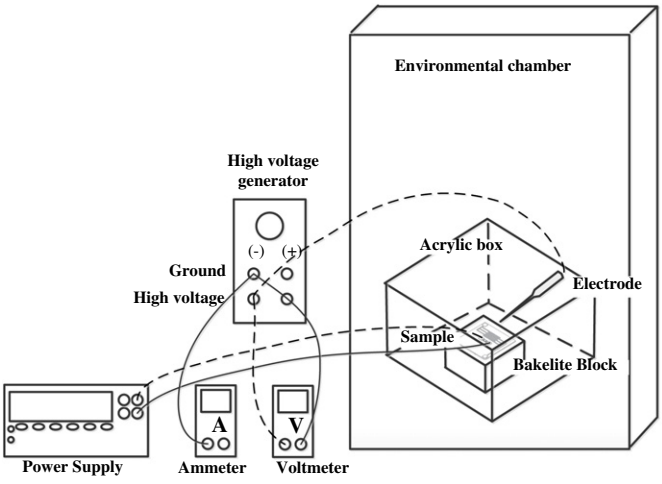

(a) Schematic of the test facility.

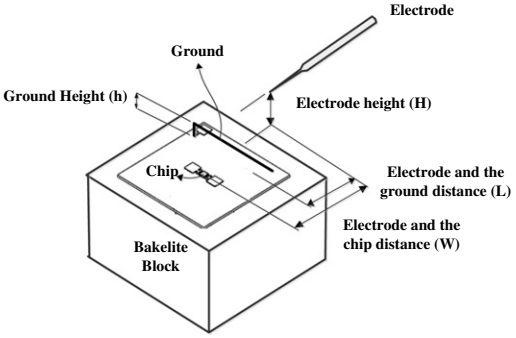

(b) Schematic of the test section.

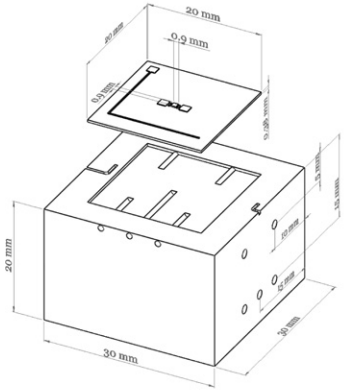

(c) Detailed dimension of the LED chip and location of the installed thermocouples.

(d) Point electrode used in this study.

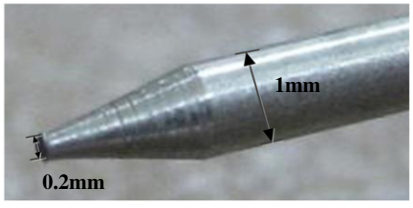

(e) Dimensions of the point electrode.

Fig. 1. Schematic of the test facility, bakelite, and the point electrode.

$(L) \times 0.5$ m $(W) \times 0.5$ m (H) was employed to carry out the experimental tests. The ambient temperature in the chamber was set to be 25 °C and RH = 60% with a controlled resolution of 0.2 °C during the experiment. To minimize the influence airflow within the environmental chamber, an acrylic housing is used to separate the controlled ambient. A power supply (GW Instek GPR-7550D) is used to power the LED and a power meter (Yokogawa WT230) is used to measure the consumed power for those LED. The LED chip size is 0.9 mm × 0.9 mm having a nominal power consumption of 1 W. Note that the corresponding efficiency of the LED, the ratio of net heat dissipation to total electric power input, is 0.75 according to the luminous efficacy of the present LEDs provided by the manufacturer and the energy balance diagram for high-power white LEDs proposed by Krames et al. [22]. The electrode is placed above the LED as shown in Fig. 1b. A thermocouple is used to measure the ambient temperature. Besides the ambient temperature measurement, additional five copper-constantan thermocouples (Omega), with their locations being represented in Fig. 1c, were used to measure the temperature of the LED chip. Notice that the maximum temperature located at the center is used to calculated the effective thermal resistance of the LED chip. The thermocouples were pre-calibrated from 20 °C to 80 °C, with a calibrated accuracy of 0.1 °C. All the measured temperatures were recorded by a data acquisition unit (Yokogawa MX100) for further heat transfer analysis. An insulation box made of bakelite with a low thermal conductivity of 0.233 W m^{-1} K^{-1} is placed beneath the heater to reduce the heat loss. In addition, a total of four T-type thermocouples are installed inside the bakelite block at two cross positions to calculate the heat loss from the bottom of the Kapton heater as depicted in Fig. 1c.

The measured average temperature in the backlite is then used to estimate the heat loss via Fourier's law of conduction. In this study, a point electrode is used for engendering the ionic wind while the ground electrodes are either point, wire, and mesh type. Notice that the point electrode is made of stainless steel of 1 mm in diameter and capped with a hemisphere tip of 0.2 mm as shown in Fig. 1d and e.

The heat dissipated of the LED (Q) is estimated as the 75% of the total power input (P) as explained earlier. The actual heat dissipated, Q_a, by convection is thus obtained by subtracting the heat loss (Q_l) from the total dissipated heat:

$$Q_a = Q - Q_l \tag{1}$$

$$Q_l = kA\frac{dT}{dx} = kA\frac{T_{ins,c1} - T_{ins,c2}}{t} \tag{2}$$

where Q_l represent heat loss from the bakelite. Hence, the thermal resistance of the LED subject to EHD is given as:

$$R_{th} = \frac{\Delta T}{Q_a} \tag{3}$$

where ΔT represents the temperature difference between LED and ambient. The uncertainty of the measured thermal resistance was ranged from 3.3% to 5.2%.

3. Results and discussion

Fig. 2a shows the effect of aligned electrode on the thermal resistance subject to the applied voltage and the corresponding

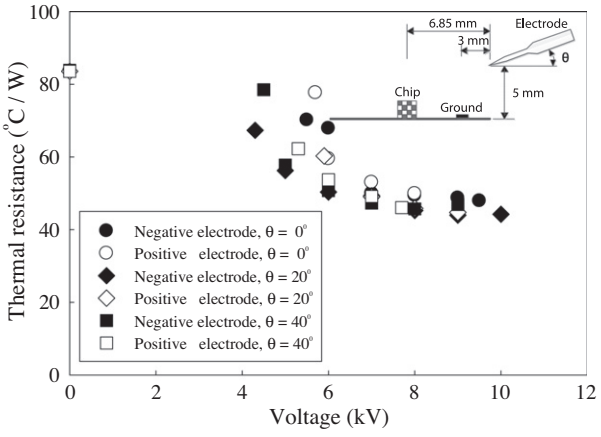

(a) Thermal resistance vs. applied voltage.

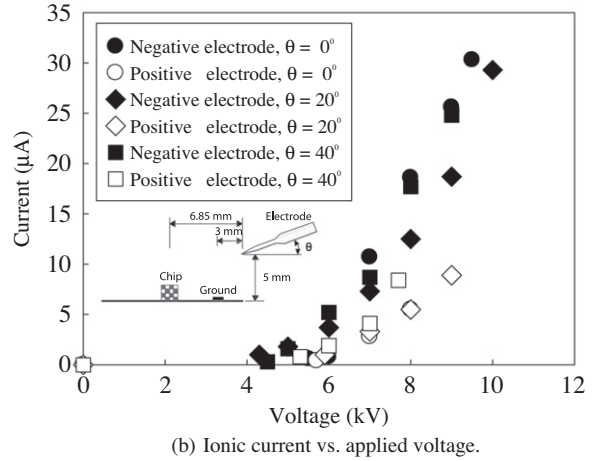

(b) Ionic current vs. applied voltage.

Fig. 2. Effect of aligned angle on the thermal resistance and the corresponding *I–V* characteristics of the LED chip.

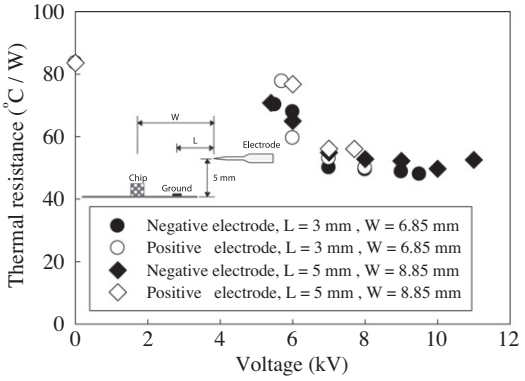

(a) Thermal resistance vs. applied voltage.

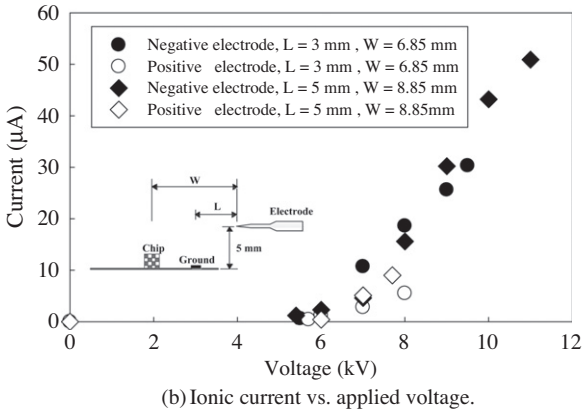

(b) Ionic current vs. applied voltage.

Fig. 3. Effect of horizontal separation distance on the thermal resistance and the corresponding *IV* characteristics of the LED chip.

variation of corona current is depicted in Fig. 2b. Note that the data with supplied voltage being 0 kV represents the base line reference where only pure natural convection is present. The height of thee point electrode is 5 mm above the LED substrate whereas the ground electrode is on the substrate having a line configuration as shown in the schematic. The aligned angle is 0°, 20°, and 40° from the horizontal orientation, respectively. Test results clearly show that the thermal resistance is appreciably reduced with the rise of the applied voltage as long as the supplied voltage pass the threshold voltage, and the maximum reduction in thermal resistance can be as high as 50% before the spark over voltage is reached. Notice that the threshold voltage is about 4 kV. This prevails for both positive and negative electrode but it is noted that the negative electrode normally shows a smaller thermal resistance than that of the positive polarity around 10% order. One of the explanations for this phenomenon is due to the higher mobility of the negative ions. Notice that the mobility of air for positive ion is 1.4×10^{-4} m^2/volt s while the negative ion is 2.0×10^{-4} m^2/volt s [23]. An indirect evidence of the better heat transfer performance for negative ion can be seen from Fig. 2b which shows that the corona current at an applied voltage for negative ion is normally higher than that of the positive ion. Since the induced ionic wind velocity is proportional to the square root of corona current [24], it therefore suggests a higher heat transfer performance of the negative polarity. On the other hand, the break down voltage for positive electrode is appreciably lower than that of negative electrode, implying a shorter operation range of the positive electrode. The results are in line with the observation by Shaughnessy and Solomon [25] who had presented *I–V* characteristics for positive and negative electrode with separation distance being 20 mm, 75 mm, and 300 mm, respectively. Their results clearly showed that the ionic current for positive electrode is appreciably lower than that of negative polarity. Yet the spark-over voltage for positive the separation distance of 20 mm is only half of the negative polarity. The measured ionic current vs. applied voltage is shown in Fig. 2b. Note that the *I–V* reveals a Townsend like behavior, i.e.

$$i = AV(V - V0) \tag{4}$$

where A is the proportional constant for Townsend like relation and V_0 is the threshold voltage. Ferreira et al. [26] also unveiled similar

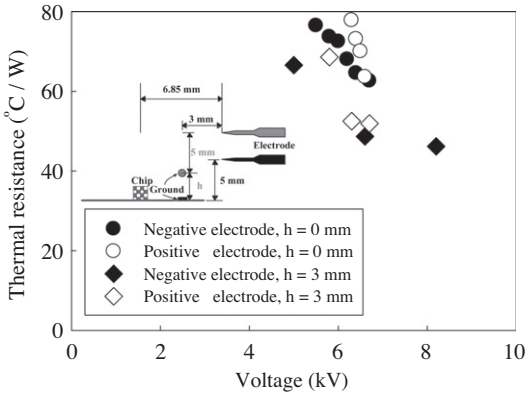

(a) Thermal resistance vs. applied voltage.

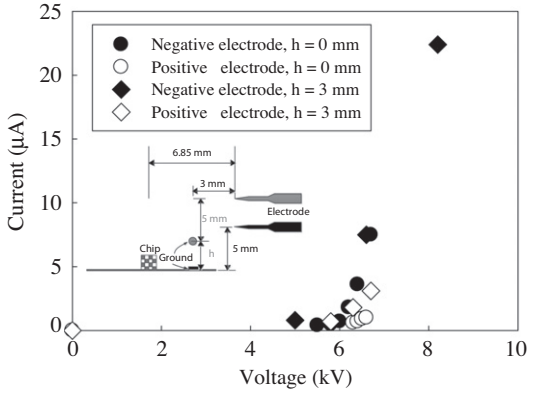

(b) Ionic current vs. applied voltage.

Fig. 4. Effect of vertical separation distance on the thermal resistance and the corresponding *I–V* characteristics of the LED chip.

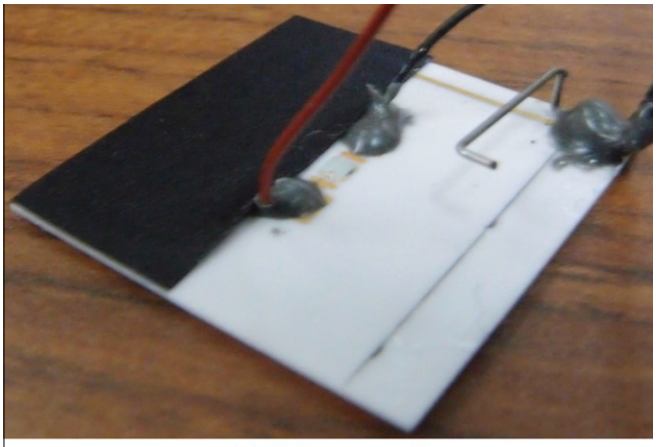

(a) Point ground

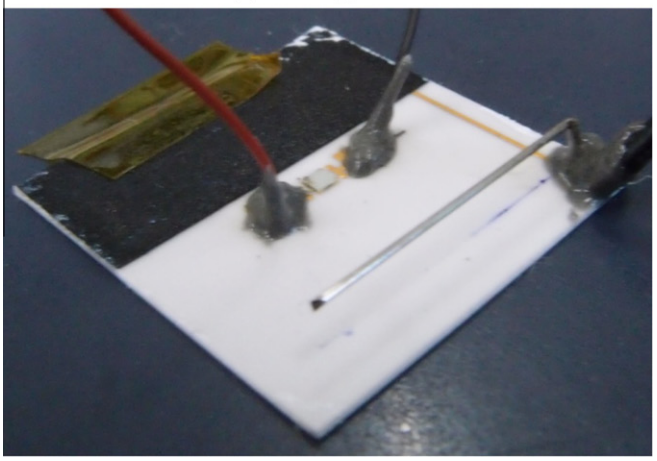

(b) Line ground

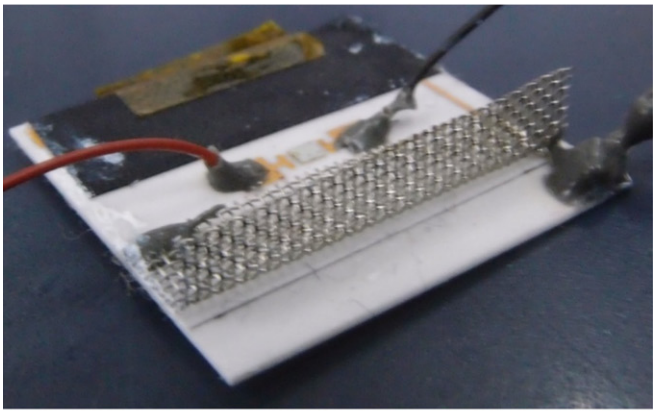

(c) Mesh ground

Fig. 5. Photo of the configuration of ground electrode – (a) point ground; (b) line ground; and (c) mesh ground.

results and the proportional constant A is related to the separation distance and normally the proportional constant for native polarity A^- exceeds than that of A^+. The value A^-/A^+ is about 1.8 when the separation distance is 15 mm. The present results for A^-/A^+ are in the order of 2 since our separation distance is less than 10 mm.

Also shown in Fig. 2a, with an increasing the aligned angle to 20° leads to an appreciable drop of thermal resistance even though the distance between the electrode and the LED is fixed. However, a further increase in aligned angle to 40° shows no further decrease in thermal resistance. The decrease of thermal resistance with the aligned angle is related to the induced airflow in which a larger induced airflow parallel to the chip is introduced. In contrast, since the ground electrode is located about 3 mm ahead of the die chip, a larger aligned angle does not appreciably increase the ionic wind component parallel to the chip direction. The airflow produced by electronic discharge in a pin-plate configuration was numerically illustrated by Zhao and Adamiak [27]. They had conducted a numerical calculation of the airflow engendering from a needle electrode normal to a plate ground. Their calculations clearly show that an apparent axial flow is induced from the electrode toward the plate ground while a radial flow component occurs near the ground plate, and a re-circulation may even exist from this radial component. With the rise of the aligned angle, it is expected that the radial component is also increasing which may contribute to reduce the thermal resistance. But on the other hand, a further rise of aligned angle also reduce the axial velocity component that acts to increase the thickness of thermal boundary layer and the possible formation of re-circulation of the radial component as shown by Zhao and Adamiak [27]. As a consequence, one can see that the thermal resistance between 20° and 40° is comparable.

The effect of horizontal separation distance of electrode on the thermal resistance is shown in Fig. 3a and the corresponding ionic current is shown in Fig. 3b. Analogously, the negative polarity also shows a lower thermal resistance than that of the positive electrode and the positive polarity shows a narrower operation range. Normally a shorter horizontal separation distance gives rise to a smaller thermal resistance due to its higher electric strength (V/m). However, the breakdown voltage is also lower for a shorter distance. The overall thermal resistance reduction is about the same for both horizontal separation distance but a longer distance provides a much larger operational range. Fig. 4 shows the effect of vertical separation distance of the electrode on the thermal resistance and its corresponding I–V characteristics. Notice that the point and ground electrode are shifted vertically by 3 mm simultaneously. In contrast to that of horizontal separation, the thermal resistance is substantially reduced subject to vertical separation. For a negative polarity of 6.7 kV, the thermal resistance for h = 3 mm is approximately 45% lower than that of h = 0 mm. The results are quite surprising for the corona current appeared in Fig. 4b is roughly the same, suggesting similar ionic wind velocities at the point electrode between h = 0 and h = 3 mm. The huge difference is actually associated with effective airflow as it flows across the LED chip. With h = 0 mm, the intensity of the induced airflow is jeopardized with the presence of substrate wall surface where no slip condition prevails. The condition is eased when h is slightly increased to 3 mm in

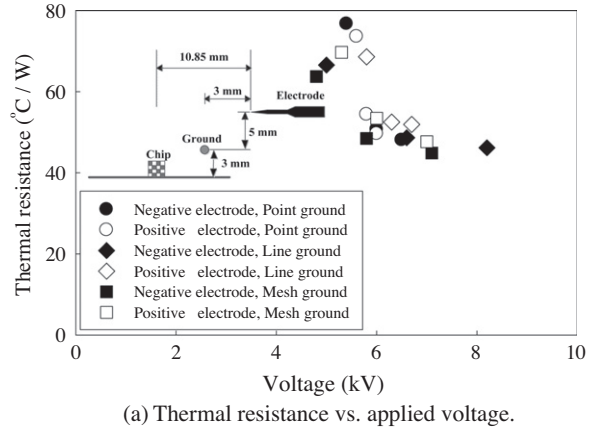

(a) Thermal resistance vs. applied voltage.

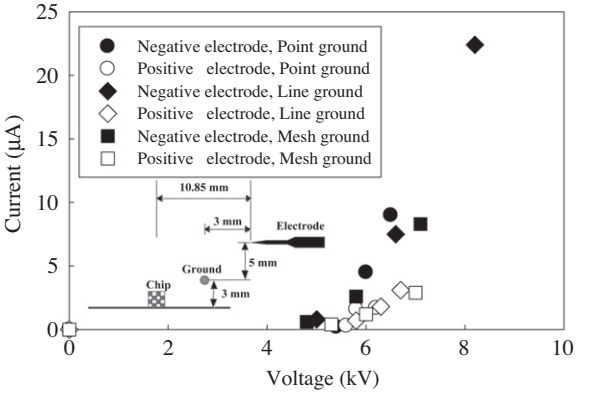

(b) Ionic current vs. applied voltage.

Fig. 6. Effect of the configuration of the ground electrode on the thermal resistance and the corresponding I–V characteristics of the LED chip.

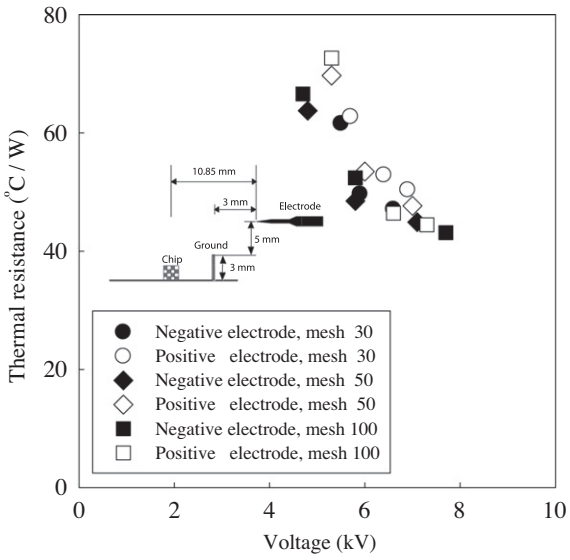

(a) Thermal resistance vs. applied voltage.

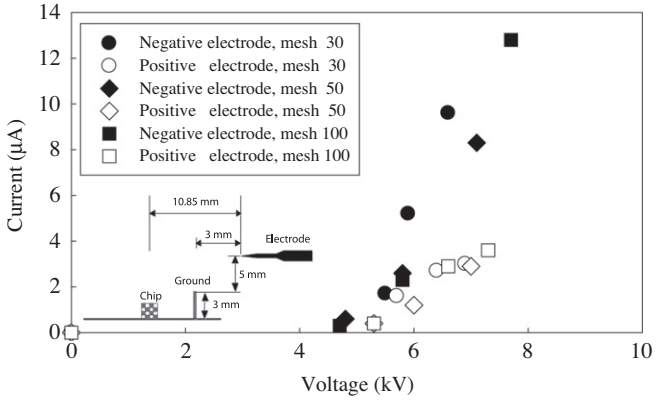

(b) Ionic current vs. applied voltage.

Fig. 7. Effect of the mesh size on the thermal resistance and the corresponding I–V characteristics of the LED chip.

which the induced jet stream does not significantly influenced by the presence of substrate surface.

The effect of the configuration of the ground electrode on the thermal resistance is also examined in this study. The ground configurations tested in this study include point, line, and mesh as depicted in Fig. 5. The corresponding measured thermal resistance and *IV* characteristics are shown in Fig. 6. Apparently, the thermal resistance for the mesh ground electrode is lowest among the three ground electrodes, followed by the line electrode, yet the point electrode shows the largest thermal resistance and the shortest operation range from the threshold to the break down voltage. The results can be interpreted from the LDA velocity measurement in a negative-to-plane corona wind by Béquin et al. [28]. They showed that whatever the geometric and electric configuration, the measured velocity decreases abruptly near the point electrode and decreases very slowly toward the mesh. On the other hand, Zhao and Adamiak [27] had conducted numerical calculation for ionic wind amid plate and mesh ground electrode. One of the interesting results they found for the mesh electrode relative to that of plate electrode is the elimination of the radial component as the airflow is approaching the ground electrode, thereby eliminating the re-circulation follow caused by the radial component. In this regard, more uniform airflow toward the mesh electrode is expected, and results in a higher heat transfer performance when a mesh ground electrode is used. For a further clarification of the effect of mesh type electrode, three mesh densities are used for testing. The nominal mesh density is mesh #30, mesh #50, and mesh #100. The mesh #30 indicates there are 30 pores per inch and so forth. The corresponding stainless wire diameter of the mesh #30, #50, and #100 are, 0.3, 0.2, and 0.1 mm, respectively. Test results shown in Fig. 7 indicates that the thermal resistance is slightly reduced when mesh 30 is changed to mesh 50. In contrast, the thermal resistance remains about the same when the finest mesh (mesh #100) is used. Despite a slight drop of thermal resistance is associated with uniform ionic velocity exerted by the mesh electrode, finest mesh is also prone to a higher frictional resistance, thereby reducing the effective induced ionic wind across the mesh electrode. As a result, no further improvement in thermal resistance is observed at the finest mesh.

4. Conclusions

This study employed ionic wind to augment heat transfer of a LED mounted on a substrate. The size of the LED die is 0.9 mm $\times$ 0.9 mm with a nominal power of 1 W. A needle type electrode is used to generate ionic wind with applied voltage ranging from 4 to 11 kV. The effects of aligned angle, electrode polarity, vertical position, horizontal position, and ground configuration on the thermal resistance of the LED substrate are examined in this study. Based on the foregoing discussions, the following conclusions are reached:

1. For the same applied voltage, it appears that the thermal resistance for the negative polarity is lower than that for the positive one within the operating voltage. The negative polarity generates a greater corona current and has a better operational range as compared with the positive one. The thermal resistance can be reduced as much as 50% in the test range.
2. The thermal resistance is slightly reduced when the aligned angle is increased from 0° to 20°, but a further increase of aligned angle casts no further reduction on the thermal resistance. This is associated with variation of radial component of the ionic wind.
3. For the effect of separation distance between electrodes, it is found that the influence of vertical separation distance is moderately pronounced than that of horizontal separation distance. This is related to the influence of the substrate surface.
4. A total of three kinds of ground electrode, including point, line, and mesh electrode are tested and compared. It is found that the mesh electrode shows a moderately lower thermal resistance than the other electrodes. The thermal resistance is slightly reduced when the mesh size is increased from #30 to #50. However, a further increase of mesh size to #100 shows no further improvement due to its higher frictional contribution.

Acknowledgments

This work is supported by the National Science Council of Taiwan under contract of 100-2622-E-009-005-CC2. The financial support from the Department of Industrial Technology and Bureau of Energy from the Ministry of Economic Affairs, Taiwan is also highly appreciated.

References

[1] F.J. Peng, C.-H. Moon, Effects of some factors on the thermal-dissipation characteristics of high-power LED packages, J. Inform. Dis. 13 (2012) 1–6.
[2] M.R. Krames, O.B. Shchekin, R. Mueller-Mach, G.O. Mueller, L. Zhou, Status and future of high-power light-emitting diodes for solid-state lighting, J. Dis. Technol. 3 (2007) 160–175.
[3] R.V. Steele, High-brightness LED market overview, Proc. SPIE 4445 (2001) 1–4.
[4] L. Kim, M.W. Shin, Thermal analysis and design of high power LED packages and systems, in: Proceedings of SPIE Sixth International Conference on Solid State Lighting, vol. 6337, 2006, pp. 25-28.
[5] N. Narendran, Y. Gu, Life of LED-based white light sources, J. Dis. Technol. 1 (2005) 167–170.
[6] J. Petroski, Spacing of high-brightness LEDs on metal substrate PCB's for proper thermal performance, in: Proceedings of the Intersociety Conference on Thermomechanical Phenomena in Electronic Systems, 2004.
[7] A. Christensen, S. Graham, Thermal effects in packaging high power light emitting diode arrays, Appl. Therm. Eng. 29 (2009) 364–371.
[8] J. Li, L. Liu, L.H. Deng, B.K. Ma, F.L. Wang, H. Lei, Interfacial microstructures and thermodynamics of thermosonic Cu-wire bonding, IEEE Electr. Dev. Lett. 32 (2011) 1433–1435.
[9] J. Li, L. Han, J. Duan, J. Zhong, Interface mechanism of ultrasonic flip chip bonding, Appl. Phys. Lett. 90 (2007) 242902.
[10] J.C. Shyu, K.W. Hsu, K.S. Yang, C.C. Wang, Thermal characterization of shrouded plate fin array on an LED backlight panel, Appl. Therm. Eng. 31 (2012) 2909–2915.
[11] S.H. Yu, K.S. Lee, S.J. Yook, Optimum design of a radial heat sink under natural convection, Int. J. Heat Mass Transfer 54 (2011) 2499–2505.
[12] X. Luo, W. Chen, R. Sun, S. Liu, Experimental and numerical investigation of a microjet-based cooling system for high power LEDs, Heat Trans. Eng. 29 (2008) 774–781.
[13] S. Liu, J. Yang, Z. Gan, X. Luo, Structural optimization of a microjet based cooling system for high power LEDs, Int. J. Therm. Sci. 47 (2008) 1086–1095.
[14] Y. Lai, N. Cordero, F. Barthel, F. Tebbe, J. Kuhn, R. Apfelbeck, D. Wurtenberger, Liquid cooling of bright LEDs for automotive applications, Appl. Therm. Eng. 29 (2009) 1239–1244.
[15] Y. Deng, J. Liu, A liquid metal cooling system for the thermal management of high power LEDs, Int. Commun. Heat Mass Transfer 37 (2010) 788–791.
[16] Z.M. Wan, J. Liu, K.L. Su, X.H. Hu, S.S. Ma, Flow and heat transfer in porous micro heat sink for thermal management of high power LEDs, Microelectronics 42 (2011) 632–637.
[17] J. Li, B. Ma, R. Wang, L. Han, Study on a cooling system based on thermoelectric cooler for thermal management of high-power LEDs, Microelectron. Reliab. 51 (2011) 2210–2215.
[18] R.J. O'Brien, A.J. Shine, Some effects of an electric field on heat transfer from a vertical plate in free convection, J. Heat Transfer 89 (1967) 114–116.
[19] A.S. Mitchell, L.E. Williams, Heat transfer by the corona wind impinging on a plate surface, J. Electrostat. 5 (1978) 309–324.
[20] B.L. Owsenek, J. Seyed-Yagoobi, R.H. Page, Experimental investigation of corona wind heat transfer enhancement with a heated horizontal flat plate, J. Heat Transfer 119 (1995) 309–315.
[21] W.J. Sheu, R.T. Huang, C.C. Wang, Heat transfer enhancement by needle-arrayed electrodes - an EHD integrated cooling system, Energy Convers. Manage. 50 (2009) 1789–1796.
[22] M.R. Krames, O.B. Shchekin, R. Muller-Mach, G.O. Muller, L. Zhou, G. Harbers, G. Craford, Status and future of high-power light-emitting diodes for solid-state lighting, J. Dis. Technol. 3 (2007) 160–175.
[23] O.M. Stuetzer, Ion drag pressure generation, J. Appl. Phys. 30 (1959) 984–994.
[24] M. Robinson, Movement of air in the electric wind of the corona discharge, Trans. AIEE 80 (1961) 143–150.

[25] E.J. Shaughnessy, G.S. Solomon, Electrohydraulic pressure of the point-to-plane corona discharge, Aero. Sci. Technol. 14 (1991) 193–200.
[26] G.F.L. Ferreira, O.N. Oliveira Jr., J.A. Giacometti, Point-to-plane corona: current–voltage characteristics for positive and negative polarity with evidence of an electronic component, J. Appl. Phys. 59 (1986) 3045–3049.
[27] L. Zhao, K. Adamiak, EHD flow in air produced by electrical corona discharge in pin-plate configuration, J. Electrostat. 63 (2005) 337–350.
[28] Ph. Béquina, K. Castora, J. Scholten, Electric wind characterisation in negative point-to-plane corona discharges in air, The Euro. Phys. J. Appl. Phys. 22 (2003) 41–49.